Arabian Journal for Science and Engineering
https://doi.org/10.1007/s13369-021-05794-2

RESEARCH ARTICLE-MECHANICAL ENGINEERING

Performance Assessment of a Refrigeration System Charged with Different Refrigerants Using Infrared Image Processing Techniques

Ferzan Katircioğlu[1] · Zafer Cingiz[2] · Yusuf Çay[3] · Ali Etem Gürel[4] · Ahmet Kolip[3]

Received: 11 February 2021 / Accepted: 29 May 2021

Abstract
This study aims to investigate the performance of R417A, R422A, R422D and R438A refrigerants as alternatives to R22, in a commercial type refrigeration system operating with R22 refrigerant. To this end, first of all, the cooling capacity and coefficient of performance (COP) values were calculated for all refrigerants used in the experimental setup. Then, two methods were proposed, Pearson's Correlation Similarity Analysis (PCSA) and surface temperature-based COP (COP_{ST}), to evaluate the success of each alternative refrigerants, and R22 with infrared image analysis, separately. The COP values obtained for the refrigerants with the mathematical method are R22 4.07, R438A 3.88, R417A 3.63, R422D 3.37, and R422A 3.18, respectively. Both the COP values and the PCSA values (R438A 0.9425, R417A 0.9343, R422D 0.9167 and R422A 0.9080) show the proximity between the R22 refrigerant and other refrigerants. Similarly, the COP_{ST} method revealed the values of R22 6.8865, R438A 5.9539, R417A 5.3273, R422D 4.9898 and R422A 4.3057, and the fact that it has the same order with the other two methods demonstrates its operability in the performance test application with the developed infrared image processing. The compatibility of the order in the experimental results obtained from the PCSA and COP_{ST} methods and the COP calculation method and has proved that thanks to infrared imaging, the remote performance analysis of the refrigeration system can be successfully performed.

Keywords Ozone depletion potential (ODP) · Global warming potential (GWP) · Infrared image processing · Pearson's correlation similarity analysis · Coefficient of performance (COP)

1 Introduction

Humans have always needed both heating and cooling technologies for the continuation of their daily life. Therefore, in order for human beings to continue their lives comfortably in the environments they live, these places must be heated, cooled and also air-conditioned. Refrigeration technologies are one of the technologies used in the creation of comfortable living spaces, in the preservation of food and in other areas of life. This situation has increased the studies on the development of refrigeration technologies every day.

R22 refrigerant is used in many air conditioning and refrigeration systems. Ozone depletion potential (ODP) is greatly increased as a result of the release of this refrigerant from existing devices due to malfunction or displacement. As R22 is the most common refrigerant currently used for commercial, domestic and industrial applications, its phased removal is expected to directly affect many systems around the world. Therefore, replacing these systems with alternatives of R22 may minimize the usage problem that can arise.

If the R22 refrigerant is made obsolete, the commercial refrigeration industry has three types of solutions. First, it is recommended not to use the older systems again as they have reached the end of their lifespan. This solution involves a pure exchange of the refrigerant without any changes in the

✉ Ali Etem Gürel
etemgurel@gmail.com

[1] Department of Electronic and Automation, Düzce Vocational School, Düzce University, Düzce, Turkey

[2] Department of Electricity and Energy, Düzce Vocational School, Duzce University, Düzce, Turkey

[3] Department of Mechanical Engineering, Faculty of Technology, Sakarya University of Applied Sciences, Sakarya, Turkey

[4] Department of Mechanical Engineering, Faculty of Engineering, Duzce University, Düzce, Turkey

Published online: 18 June 2021

refrigeration system and preserving the existing lubricating oil. The second option is to do a retfofit. This is understood as an active adaptation to the new refrigerant, which may include the replacement of the refrigeration system, lubricating oil, expansion valves and other elements of the system. Finally, if possible, a good solution would be to design new systems using long-term refrigerants such as hydrocarbons, ammonia or carbon dioxide for the new equipment. When the literature is reviewed, it is seen that various studies have been conducted on R22 refrigerant and its alternatives. Aprea et al. used R417A instead of R22 in their vapor compression refrigeration system. The results showed that the COP of R417A was 14% lower than that of R22 and the exergy breakdown of R417A was 14% higher than that of R22 [1]. Torella et al. performed an energy performance study on R22 water cooler when R22 was renewed with R417A and R422D. The results indicated that the evaporator and condenser temperatures were different for both refrigerants, and when working with other refrigerants, there was a decrease in refrigeration capacity, compressor power, energy consumption and discharge temperature [2]. La Rocca et al. compared R22, R417A, R422A and R422D refrigerants to determine the performance of a vapor compression refrigeration system. According to the experimental study results, the highest TEWI values were obtained for R422A, R422D, R417A and R22 refrigerants, respectively. In addition, it has been shown that major system modification is not necessary; however, there is an improvement in energy efficiency [3]. Elgendy et al. compared R22 with R438A. System performance has been evaluated under mass flow and different condensation temperature conditions. For the system using R22 refrigerant, a COP value between 1.63 and 1.93 was obtained, while the COP values were found to be between 1.46 and 1.66 when R22 was replaced with R438A refrigerant [4]. Saeed et al. evaluated the performance of refrigerants with zero ODP value by exchanging them with refrigerants including R407C, R417A, R422D, R427A and R438A and making energy and exergy analysis. COP and exergy efficiency show that none of the refrigerants selected is as efficient as R22; however, the values show that each refrigerant can be considered as a potential alternative for retrofit [5] Ergün et al. examined the thermodynamic aspects of R417A and R438A, an alternative to the widely used R22 refrigerant. The performances of R22, R417A and R438A refrigerants have been compared. Their study revealed that R438A refrigerant had higher COP_h and COP_C values than R417A and R438A refrigerants developed as an alternative to R22 refrigerant [6]. Cingiz et al. investigated the performance of R417A, R438A, R422A and R422D refrigerants instead of R22, which is widely used in refrigeration systems, according to the first and second law of thermodynamics. The COP value of the refrigeration system using R22 was taken as a reference and it was compared with the COP values of other refrigerants. It has been observed that the refrigerants that gave the closest results to R22 were R438A, R417A, R422D and R422A, respectively [7].

Refrigerants that have recently been added to the list as an alternative to R22 are R422A, R422B, R422C and R422D. The report published by the American Environmental Protection Agency has indicated that these refrigerants can be used in home and commercial applications [8]. To determine the COP of air conditioners, it is necessary to measure the temperatures and pressures in the system. The calculation process takes a long time. Erham et al. designed a COP monitoring system to solve this problem. It has been predicted that the use of the proposed method can help save 2 h (80% saving) [9].

Infrared thermography is mainly used in military security, forestry, medicine, maintenance of mechanical and electrical systems, search and rescue and building maintenance. Using infrared cameras, several studies have conducted building diagnostics, energy audits, or detection of insulation faults of the heating, ventilating and air conditioning (HVAC) systems [10–15]. Carignano et al. investigated the defrosting of the windshields of industrial vehicles with computer-assisted thermographic analysis [16]. Burch et al. examined infrared thermography for automotive air conditioning control analysis and also proposed a solution for measuring ambient air temperature using a thin-layer fiberglass screen mounted vertically in the air stream [17]. In another study, using a thermal camera, results and analysis of the thermal performance of a flat plate heat pipe were presented. The steady-state and transient temperature distribution of the evaporator surface of the flat plate heat pipe was measured using a single heat source with various heat flux inputs [18]. Freund et al. applied the infrared thermography method to a spray refrigeration system to measure local heat transfer coefficients. This technique, which is based on infrared temperature measurements and the finite difference model of the wall, enabled a rapid and fluid-independent evaluation of the heat transfer coefficient of a heat transfer wall [19]. In their study, Korukçu et al. used an infrared thermal camera with a spectral range of 7.5 to 13 μm to capture infrared thermography of surfaces. Instantaneous and temporary temperature distributions of all surfaces inside an automobile were determined, and the thermal disturbances caused by these surfaces were investigated [20].

The advantages of thermal imaging are speed in milliseconds, simplification of the measurement of moving targets, procedures without contact, examination of the temperature properties of dangerous or physically inaccessible objects, no energy loss at the target, and no mechanical impact on the surface of the object. All these factors have sparked the interest in infrared technologies for new types of applications and users [21, 22]. Weinmann et al. used thermal images to identify insulation defects in pipes and buildings

[23]. Righetti et al. carried out a comparative performance analysis of HFO1234yf, HFO1234ze and HC600a low GWP refrigerants in roll-bond evaporators for household refrigerators. To carry out the analysis, two thermocouples and a thermal camera placed at the back of the roll-bond evaporator were used. Infrared images obtained with the thermal camera were used to monitor the surface temperature of the roll-bond evaporator and to verify thermocouple measurements during the experimental test period [24]. A state monitoring system and intelligent diagnostics were proposed to classify the different states of cooling radiators using infrared thermal images. The proposed study consisted of a series of procedures including thermal image acquisition, image processing, two-dimensional discrete wavelet transform (2D-DWT), feature extraction, feature selection using genetic algorithm and finally classification using artificial neural networks [25]. A quasi-experimental model was presented to predict the refrigerant and lubricant status in both the micro-channel condenser and the plate and fin evaporator of an air conditioning system. An infrared image processing system which sees the system was used [26]. Katırcıoğlu et al. proposed improving the thermal images in order to compare the performance of different refrigerants without remote sensors with thermal image analysis in refrigeration systems. The experimental results revealed that the proposed algorithm not only increased the contrast and detail information, but also obtained a clear image by providing blur reduction [27]. Kim used a thermal camera to detect methane gas leaks. Necessary information was provided for the detection of invisible gas leakage with adaptive histogram equalization and averaging operations of the rear part of the image [28]. In the study carried out by Katırcıoğlu, infrared imaging and remote sensing application was developed for greenhouse systems. It has been proposed to obtain average temperature and air relative humidity in the greenhouse with infrared imaging and the psychrometric diagram application, and soil moisture values using the multiple regression analysis method [29].

In order to determine the COP of refrigeration and air conditioning systems, it is necessary to measure the temperatures and pressures on the system. The process takes a considerable amount of time since the COP is found through value calculation. The reason for this is that measurements at many different points are made one by one. In addition, in order to calculate the COP, it is necessary to find the enthalpies determined according to the temperature and pressure values in the P-h diagram. Next, the enthalpy values found for the COP are placed in the formulation. It is important to determine the COP by using alternative methods in order to reduce the loss of time and minimize the error rate.

As a result of the studies conducted for commercial refrigeration systems and infrared image processing, to the best of the authors' knowledge, there are no studies in which two systems are applied together, heretofore. Infrared thermography is a more convenient and faster method than normal temperature measurement methods. In this study, using infrared thermal image processing methods, investigating the COP performance of R22, R417A, R438A, R422D and R422A refrigerants in commercial type refrigeration systems and surface temperature-based COP calculation method is proposed.

2 Material and ve Method

2.1 Experimental Setup

The experimental system is designed on the basis of the vapor compression refrigeration cycle. A commercial type refrigeration system operating with R22 refrigerant and R438A, R417A, R422D and R422A refrigerants examined as alternatives to R22 in the experimental system was manufactured. The general view of the experimental rig is given in Fig. 1.

Each refrigerant to be tested was charged as 900 g, the compressor was cleaned with nitrogen before charging and vacuuming was performed. In order to be able to perform the experiments in a stable environment and to examine the performances of different refrigerants in a more realistic way, the experiments were carried out in a closed environment with a constant outside temperature. T_{in} was assumed as 21 °C (ambient temperature). In order to protect the thermal camera from different disturbing light effects, the windows of the laboratory were arranged in a way that they do not receive daylight. The lighting system of the laboratory was turned on and a constant lighting was provided. In addition, in order to evaluate the performance of the refrigeration system and five different refrigerants using image processing method, images were repeatedly taken from the system three times for each refrigerant with a thermal camera. Tests were

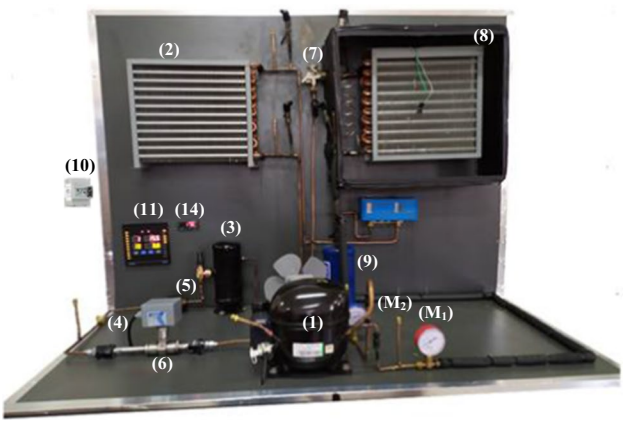

Fig. 1 General view of the experimental rig

carried out after stable operating conditions were reached. Images were taken with a thermal camera after the system become stable for one hour, while the system was working with each refrigerant.

For the measurement of temperatures in the system, instantaneous measurements were made with K-type thermocouples connected to the inputs and outputs of each main element of the system Pressure measurements were carried out with pressure transmitters. Four pressure transmitters are connected to the condenser and the inlet and outlet of the evaporator. In order to measure the volumetric flow rates of the studied refrigerants, a turbine-type flow meter was placed at the condenser outlet and the volumetric flow rate was measured and recorded. The system was used with an energy analyzer to measure the power consumption of the compressor and other electrical components. The positions of all components and measurement equipment used in the designed test system are given in Fig. 2, and their technical specifications are given in Table 1.

The tests were carried out after steady operating conditions were reached. The pressure and temperature values at the main points of the system were taken experimentally and read for each refrigerant tested. Then, the thermodynamic properties of each refrigerant tested were analyzed using Engineering Equation Solver (EES). The process of taking infrared images from the refrigeration system is given in Fig. 3. While the system was working with each refrigerant, images were taken with a thermal camera after the system became stable for one hour.

Infrared images taken from the refrigerants used in the proposed study are given in Fig. 4. They were presented with their original structure as taken from the thermal camera and before cutting and segmentation.

3 Refrigerants

In this study, R22, R43A, R417A, R422D and R422A refrigerants were used. R22 is suitable for a wide variety of refrigeration and air conditioning applications at a various temperatures. For this reason, it has become the most common refrigerant in many applications after the removal of chlorofluorocarbons (CFCs) [30]. R422D is used in multi-dimensional R22 replacement applications in direct evaporation equipment. In most systems, it shows similar performance and efficiency with R22 [31]. R417A is used instead of R22 in direct expansion constant air conditioning and medium temperature refrigeration systems [32]. R422A is used as an alternative to R22 in some low temperature commercial refrigeration applications. Field trials have shown that its energy efficiency can be better than that of R22. It provides lower pressure refrigerant temperatures compared to R22 and can extend the service life of the compressor [31].

R438A, the final refrigerant used in the experimental system, is used for R22 replacement in direct evaporation systems [31]. R438A provides similar refrigeration performance and energy efficiency to R22 when operating at a lower compressor discharge temperature, similar evaporator and condenser pressures. In the existing R22, DX refrigeration and air conditioning systems, replacement has been successfully achieved by using R438A as a refrigerant [33]. The compositions and basic thermodynamic properties of the five refrigerants used in the experimental system are given in detail in Table 2.

3.1 Method

3.1.1 Determination of the Refrigeration System Performance with the Calculation Method

The performance analysis of the system was carried out based on the first law of thermodynamics. In the first law analysis of the refrigeration system, condenser, evaporator and compressor capacities were calculated respectively by means of the following equations considering the cycle points [7].

Compressor capacity (kW) can be calculated as follows:

$$\dot{W}_{\text{comp}} = \dot{m}\left(h_2 - h_1\right) \tag{1}$$

The electrical power of the compressor is obtained by dividing the compressor capacity by electrical and mechanical efficiencies [34].

$$\dot{W}_{\text{comp,el}} = \frac{\dot{W}_{\text{comp}}}{\eta_{\text{el}} \times \eta_{\text{mec}}} \tag{2}$$

The condenser capacity (kW) of the refrigeration system can be obtained as follows:

$$\dot{Q}_{\text{cond}} = \dot{m}\left(h_2 - h_3\right) \tag{3}$$

Similarly, evaporator capacity (kW) of the refrigeration system can be calculated using Eq. (4).

$$\dot{Q}_{\text{evap}} = \dot{m}\left(h_1 - h_4\right) \tag{4}$$

The coefficient of performance (COP) of the refrigeration system is calculated as follows:

$$\text{COP} = \frac{\dot{Q}_{\text{evap}}}{\dot{W}_{\text{com,el}}} \tag{5}$$

In Eqs. (1–5), h is the specific enthalpy (kJ/kg) and $\dot{m}$ is the refrigerant flow rate (kg/s). COP is the amount or measure of the efficiency of the refrigeration system determined by the ratio of the energy consumed in the compression process to the energy absorbed in evaporation. The less

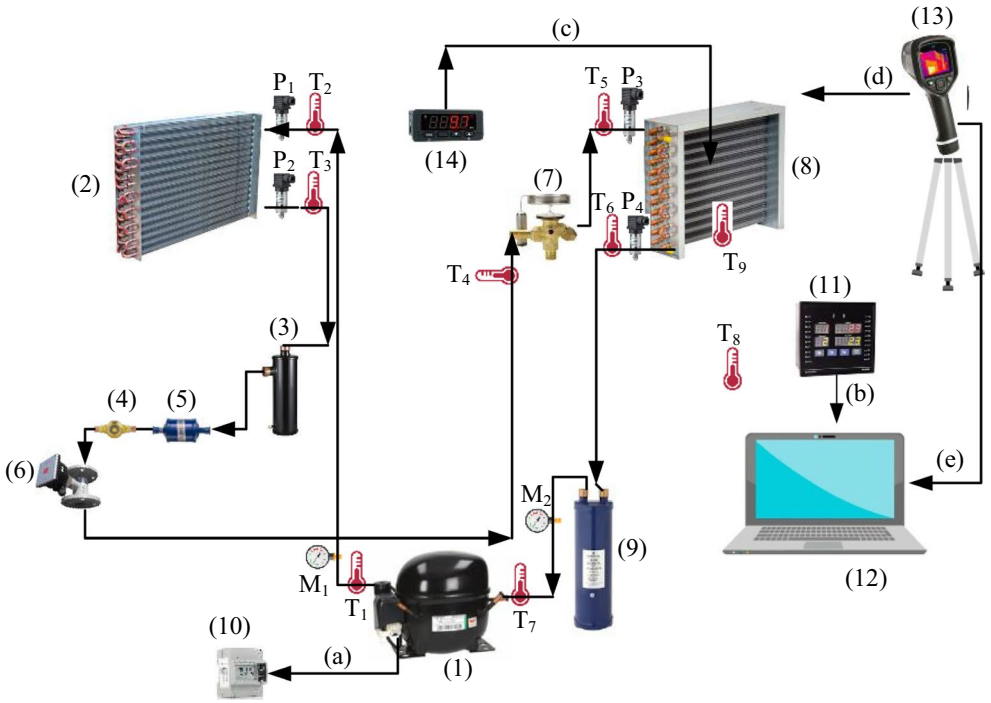

Component/measurement equipment

1	Compressor	P_1	Condenser inlet pressure sensor	12	PC
2	Condenser	P_2	Condenser outlet pressure sensor	13	Thermal camera
3	Liquid tank (receiver)	P_3	Evaporator inlet pressure sensor	14	Digital thermostat
4	Sight glass	P_4	Evaporator inlet pressure sensor	a	Energy consumption measurement
5	Drayer	T_1	Thermocouple (Compressor outlet temp.)	b	Browser data transfer
6	Flowmeter	T_2	Thermocouple (Condenser inlet temp.)	c	Thermostat evaporator connect
7	Thermostatic expansion valve	T_3	Thermocouple (Condenser outlet temp.)	M_1	Manometer (High pressure)
8	Evaporator	T_4	Thermocouple (TGV inlet temp.)	M_2	Manometer (Low pressure)
9	Refrigeration accumulator	T_5	Thermocouple (Evaporator inlet temp.)	d	Image acquisition thermal camera
10	Energy analyzer	T_6	Thermocouple (Evaporator outlet temp.)	e	Data transfer
11	Scanner and alarm device	T_7	Thermocouple (Compressor inlet temp.)		
		T_8	Thermocouple (Ambient temp.)		
		T_9	Thermocouple (Cooling cabin int. temp.)		

Fig. 2 Measurement equipment positions for the experimental system

energy consumed in the compression process, the higher the efficiency coefficient COP of the refrigeration system. Therefore, the refrigerant with the highest COP should be selected among the refrigerants with other equal characteristics and factors.

3.1.2 Refrigeration System Performance Comparison with the Pearson's Correlation Similarity Analysis (PCSA) Method

Similarity measures are the functions used to calculate the degree of similarity between objects. The degree of similarity is in the range of [0, 1] or [− 1, 1]. If it is 1, we

Table 1 Features of equipment and sensors used in the experimental setup

Equipment and Sensors	Voltage	Current	Technicial Specifications
Compressor	220–240 V		Embraco NEU 6215 GK—Hermetic reciprocating, Power: ½ HP
Condenser	220–240 V		Karyer KT- air flow, 3/4 HP
Evaporator	220–240 V		Karyer KT- air flow, 1/2 HP
Expansion valve			DuNan TGV TIS with balanced external union, One way PS 46 bar, Refrigerants: R22, Working range: -40/ + 10 °C
Liquid receiver			ESS-LRY Pressure: 32 bar, Working range: 0/ + 70 °C, Volume: 1.1 L
Liquid holder			SAN XIN SX-204
Drayer			Sanhua DTG, Welding, Working range: -40/ + 120 °C
Sight glass			SARCOOL Welding
Converter			Ordel- SBA200- USB-RS485 USB 1.1 ve 2.0 Compatible PC Connection
Process monitoring record and control program			Ordel OPİK16 Standard MODBUS RTU communication protocol Parameters can be monitored, changed and saved via computer, 128 channels can be defined to one parameter, each channel can be viewed digitally, analog and graphically,
Universal input scanner and alarm device	100–240 V AC/DC		Ordel SCN100-03/0/2/0/11 Number of inputs: 20, 2 4 Digit Numeric and 2 2 Digit Numeric Display, 22 LED Display Accuracy: ± 0.2% Universal Sensor Input (TC, RT, mA, mV, V)
Refrigerant charging station	220 V		C.E.S. Refrigerant charging station with digital scales Vacuum pump (3 m^3/h), Scale precision: ± 5 g Operating temperature: 8- 49 °C between, Pressure Gauge: 15- 30 bar
Thermal camera	AC adapter 90–260 V AC input 5 V DC output to camera		FLIR E8-XT, Infrared resolution (IR): 320 × 240 (76,800 pixels) Thermal sensitivity: < 0.05 ºC/ < 50 mK Minimum focal length: 0.5 m, Thermal sensitivity: < 0.06 ºC, Object temperature range: -20/ + 550 ºC Accuracy: ± 2 C or ± 2% of reading for ambient temperature between + 10 ºC and + 35 ºC and object temperature above + 0 C
Flow meter	12–24 V DC	4–20 mA	Bass- TDSS.004.015.D.A.10.S.S.N.N, Measuring range: 0,6… 4,5 l/dk, Precision: % 1 T.S., Temperature: -40…120 °C
Pressure transmitter	8-28 V	4–20 mA	Keller PA-21Y, for cooling groups, pressure range: 0–30 Bar Precision: %1, Operating temperature: -20…. + 85 °C
Thermocouple			Ordel KTTE2 × 0,5 T 2 K- K Type, Section: 2 × 0,5 mm^2 Single stranded, welded end, Insulation:Teflon + Teflon, Cable length:2 m
Energy analyzer	220 V	20 mA	CET PMC-220 Single phase submersible meter, 1 phase direct connection up to 63 A, 20 mA measuring start current
Thermostat	230 V AC		EVCO- EVKB 21- Digital Hold with defrost NTC: -40/ + 105 °C, Relay output: 1 Adet 16 A, Digital input: 1

understand that there is complete similarity between the two objects, while 0 [0, 1] or − 1 [− 1,1] indicates complete dissimilarity [35]. Correlation is the most commonly used measure of similarity in determining the direction and strength of the linear relationship between the attribute values of two objects [36]. The Pearson correlation between x and y data sets is calculated using the following equation, where n is the total number of objects, σ_x and σ_y are the standard deviations of the sequences, and $\bar{x}$ and $\bar{y}$ are the arithmetic mean of the sequences.

$$\text{PearsonCorr}_{xy} = \frac{\sum_{i=1}^{n}\left(x_i - \bar{x}\right)\left(y_i - \bar{y}\right)}{(n-1)\sigma_x\sigma_y} \tag{6}$$

In the proposed study, two feature matrices are entered into Pearson correlation for each cut image part from thermal images taken from systems including the reference refrigerant and the refrigerant to be compared. For each part, eight attribute values were used, namely standard deviation, entropy, contrast, skewness, maximum, minimum, average and the most intense surface temperature value.

Fig. 3 Image acquisition from the experimental rig with a thermal camera

Feature extraction from the studied image is an important step for image analysis and decision processes. It is possible to collect the feature extraction methods in images under three main headings as color, texture and shape. In the proposed study, more emphasis was placed on color and texture due to the use of infrared images. After selecting the desired regions on the infrared image, the features given below are obtained in order.

3.1.2.1 Standard Deviation In digital image processing applications, histogram is widely used to show the relationship between image level and statistical probability [37]. The value that gives the information about how far from or close to the mean each pixel in the image is collected is called standard deviation.

$$\sigma_g = \sqrt{\sum_{g=0}^{L-1} \left(g - \overline{g}\right)^2 P(g)} \tag{7}$$

$P(g)$ in Eq. (7) is the first-order histogram probability of the image and it is defined as follows:

$$P(g) = \frac{N(g)}{M} \tag{8}$$

here M is the total number of pixels in the image, and $N(g)$ is the number of pixels in the g color tone. $\overline{g}$ in Eq. (8) is the average value of the image and it is found as in Eq. (9) [38].

$$\overline{g} = \sum_{g=0}^{L-1} gP(g) \tag{9}$$

3.1.2.2 Entropy Entropy is used to measure the uncertainty in a variable. When all values of the variable are equal, there is no uncertainty and the entropy value will be zero. However, if the variable takes completely different values, entropy reaches its maximum value [39].

$$Entropy = -\sum_{g=0}^{L-1} P(g) \log_2 \left(P(g)\right) \tag{10}$$

3.1.2.3 Contrast Contrast is the difference between the lightest and darkest areas of the image. The high contrast image has both areas of very strong light and areas of very dark shadows. As a measure of global contrast, Michelson equation was used and it is expressed as in Eq. (11) [40].

$$C = \frac{L_{\max} - L_{\min}}{L_{\max} + L_{\min}} \tag{11}$$

In the equation, C represents the global contrast value, while the maximum and minimum luminance are denoted with $L_{\max}$ and $L_{\min}$, respectively.

3.1.2.4 Skewness Color information is one of the most important features of infrared images. After determining the selected zone area, the skewness value is found as in Eq. (12). The pixel color values within the selected region are not symmetrical. Therefore, skewness shows how far the average used can be far from the symmetrical property.

$$\gamma_i = \left(\frac{1}{N}\sum_{j=1}^{N} \left(f_{ij} - \mu_i\right)^3\right)^{\frac{1}{3}} \tag{12}$$

The f_{ij} value in Eq. (12) denotes the color value of the j. image pixel in channel i.; μ_i is the average value of color in channel i.; N represents the total number of pixels in the image; and γ_i is the skewness value in each channel.

3.1.2.5 Maximum and Minimum Surface Temperature The maximum and minimum temperature values of the area cut to be worked on create the feature data required for analysis. The methods of obtaining the maximum and minimum temperature data are presented in Eq. (13).

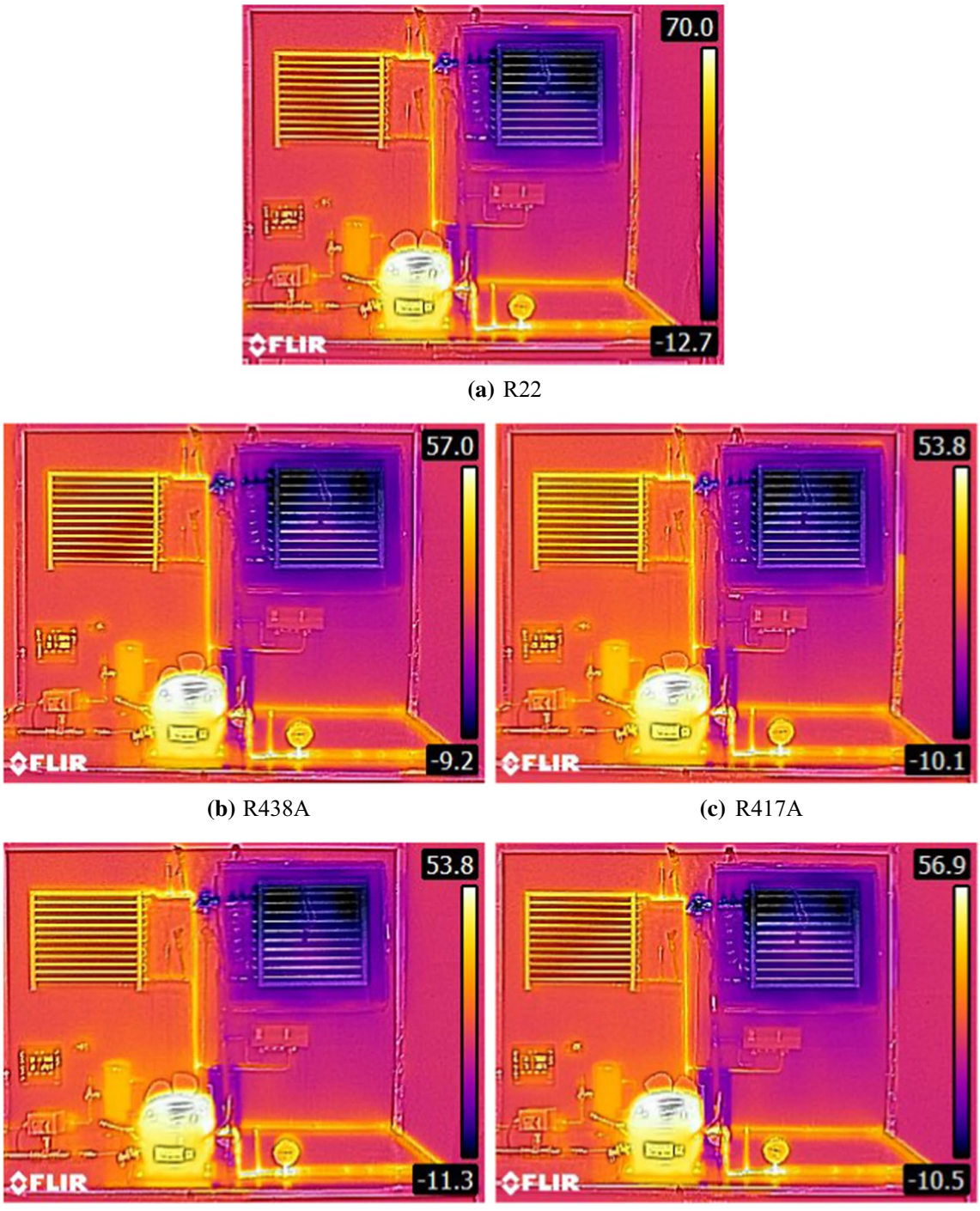

(a) R22

(b) R438A

(c) R417A

(d) R422D

(e) R422A

Fig. 4 Infrared images of the refrigerants used in the proposed study

$$T_{\max} = \max\left(T_{\text{low}} + \left(T_{\text{high}} - T_{\text{low}}\right) * T\_I\right)$$
$$T_{\min} = \min\left(T_{\text{low}} + \left(T_{\text{high}} - T_{\text{low}}\right) * T\_I\right) \quad (13)$$

T_I in Eq. (13) shows the input image obtained by converting the colored infrared image to gray thermal image, and T_{low} and T_{high} indicate the lower and upper values of the temperature bar.

3.1.2.6 Average Surface Temperature The average temperature value of the specified region in the infrared image is given in Eq. (14).

Table 2 Physical and environmental properties of tested refrigerants [7]

Property	R22	R438A		R417A		R422D		R422A	
Refrigerant composition (Mass %)	R22	R125	45%	R125	46.60%	R125	65.1%	R125	85.1%
		R134a	44.2%	R134a	50%	R134a	31.5%	R134a	11.5%
		R600	1.7%	R600	3.4%	R600a	3.4%	R600a	3.4%
		R601a	0.6%						
		R32	8.5%						
Molecular mass (kg/kmol)	86.5	99.1		106.8		109.9		116	
Critical temperature (°C)	96.2	85.3		87.1		79.6		71.7	
Critical pressure (bar)	49.9	43		40.45		39.18		37.54	
Lubricant	MO	MO/AB/POE		MO/AB/POE		MO/AB/POE		MO/AB/POE	
ODP	0.05	0		0		0		0	
GWP	1810	2264		2346		2730		3140	

MO: mineral oil, AB: alkaline benzene, POE: polyol ester

$$T_{\text{av}} = \frac{\sum_{i=1}^{M}\sum_{j=1}^{N} T_{\text{low}} + \left(T_{\text{high}} - T_{\text{low}}\right) * T\_I}{M * N} \tag{14}$$

M and N in Eq. (14) show the size of the cut area.

3.1.2.7 The Most Intense Surface Temperature Value Algorithm 1 was used to determine the most intense temperature value of the specified region in the infrared image.

expansion valve inlet, evaporator inlet–outlet) of the system and the temperatures on the surface of the compressor, condenser and evaporator were obtained with a thermal camera from specified points on the system and compared. The process of taking infrared images from the refrigeration system is given in Fig. 5 according to the regions. The regions to be used in the proposed method are numbered and the region names are also given on the figure. The feature matrices

Algorithm 1. Verbal code for determining the most dense surface temperature value.

Step 1. Find the temperature value corresponding to each pixel.

$$T\_Im = T_{low} + \left(T_{high} - T_{low}\right) * T\_I$$

Step 2. The most intense surface temperature value

```
for i=1:row
  for j=1:column
      value=T_Im(i,j);
      frequency(value)=frequency(value)+1;
  end
end
```

Step 3. Show intense temperature value

```
T_intense =Max(frequency(value));
```

In Table 3, the feature matrix obtained for the 10 sub-regions in the infrared image taken for the R22 reference refrigerant is given. In order to evaluate the performance of the refrigerants, each main element inlet and outlet (compressor inlet–outlet, condenser inlet–outlet, thermostatic obtained in the above-given refrigerants are inserted into Eq. (8), and the similarity value of each selected sub-region is found. The average similarity value is found by adding the similarity values obtained for the ten sub-regions.

Table 3 Attribute matrix example obtained for each refrigerant that will enter Pearson's Correlation Similarity Analysis (The values given are for R22)

Region	X1	X2	X3	X4	X5	X6	X7	X8
1	33.068	5.723	0.506	1.189	35.375	28.669	31.982	29
2	19.907	5.554	0.588	0.157	10.389	−7.951	3.779	4
3	29.834	6.345	0.478	0.120	22.677	21.686	22.580	23
4	69.246	6.265	0.827	0.600	19.932	−12.700	15.248	20
5	56.886	5.819	0.835	1.802	6.161	−7.445	−0.096	6
6	29.895	5.999	0.686	0.288	34.468	28.515	30.421	31
7	42.132	6.221	0.824	0.993	8.307	−2.496	6.131	8
8	48.019	6.252	0.784	0.305	21.266	16.656	19.777	21
9	13.507	5.224	0.357	−0.332	68.297	61.734	63.989	62
10	46.691	6.662	0.694	0.288	35.974	35.974	35.974	36

X1: Standard Deviation (SD)
X2: Entropy (E)
X3: Contrast (C)
X4: Skewness (S)
X5: Maximum Surface Temperature (MaxT)
X6: Minimum Surface Temperature (MinT)
X7: Average Surface Temperature (AT)
X8: Most Intense Surface Temperature (IT)

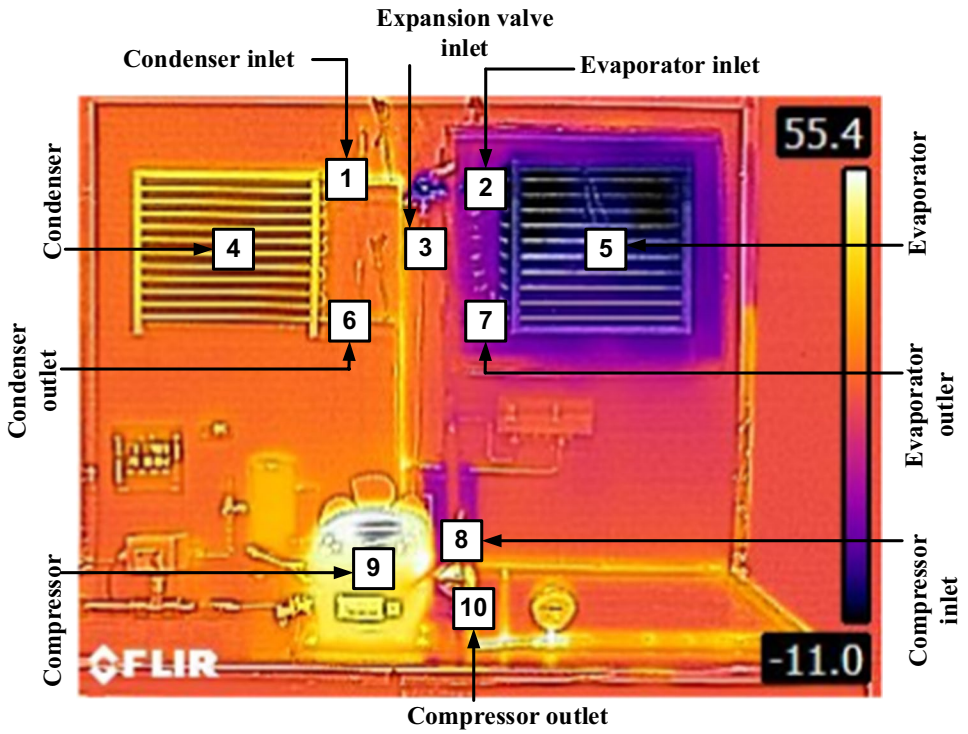

Fig. 5 Infrared image over the refrigeration system

3.1.3 COP Refrigeration System Performance Based on Surface Temperature (COP_{ST})

COP is the amount or measure of the efficiency of the refrigeration system determined by the ratio of the energy consumed in the compression process to the energy absorbed in the evaporation [41]. Inspired by the thermodynamic equations in Eqs. (2), (4) and (5) and using infrared image processing methods and surface temperature information, refrigeration system performance coefficient was proposed. The proposed COP_{ST} was named, and the abbreviation Surface Temperature (ST) was used.

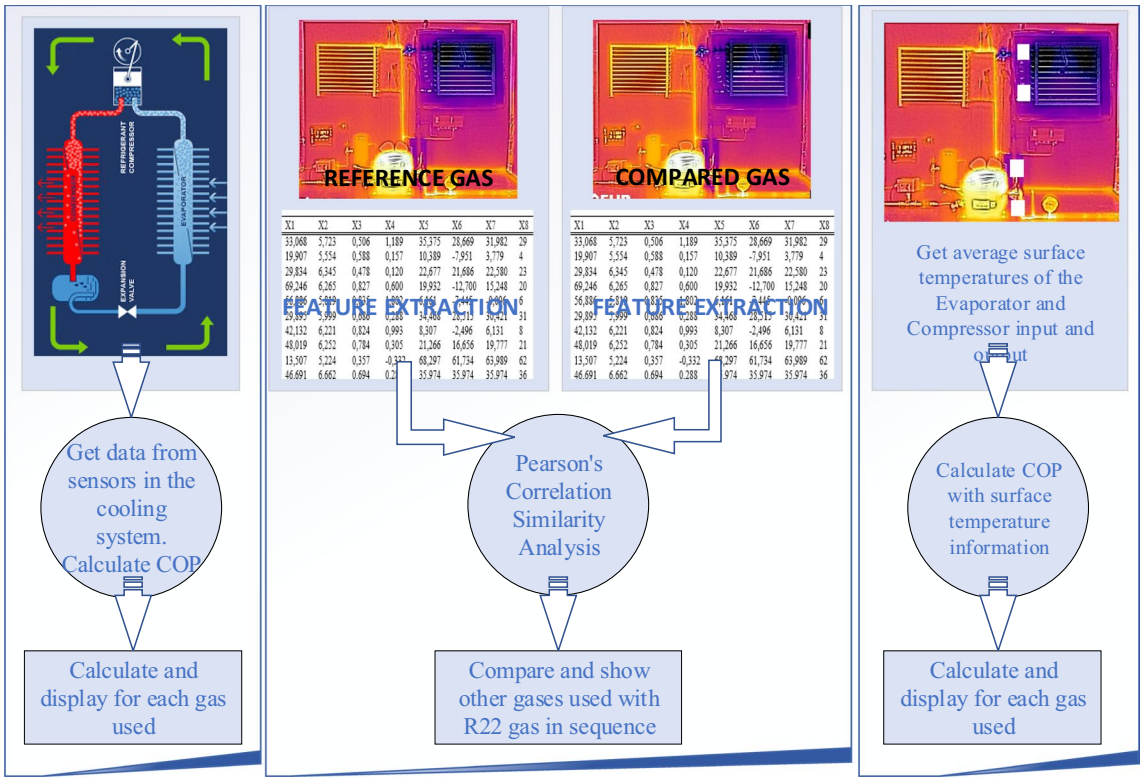

Fig. 6 Flow chart of the proposed study

$$\mathrm{COP_{ST}} = \frac{(\mathrm{Comp_{outlet}} - \mathrm{Comp_{inlet}})}{(\mathrm{Evap_{outlet}} - \mathrm{Evap_{inlet}})} \tag{15}$$

$\mathrm{Comp_{outlet}}$ and $\mathrm{Comp_{inlet}}$ in Eq. (15) represent the inlet and outlet surface temperature values of the compressor, while $\mathrm{Evap_{outlet}}$ and $\mathrm{Evap_{inlet}}$ represent the inlet and outlet surface temperature values of the evaporator. In the proposed study, after choosing the above four regions on the infrared images of the refrigerants, the values obtained are applied to Eq. (15). Average temperature value was taken as basis in the selected regions.

3.1.4 Flow Chart of the Proposed Study and Introduction of the Matlab GUI Interface

The flow chart of the proposed system is given in Fig. 6. As seen in the figure, the proposed study consists of three subsections. The first part is the reference calculation part that is widely preferred in the literature. The COP value is calculated for each refrigerant using the sensor data connected to the refrigeration system. The order of the refrigerants obtained in this section is taken as a reference for the next two sections.

In the second part, infrared images of R22 refrigerant and other refrigerants are taken with a thermal camera. In the second stage, these infrared images are added to the system in pairs, provided that they are R22 and one of the other refrigerants. Feature matrix is created for each refrigerant by extracting attribute data from the infrared images. The two property matrices are entered into the PCSA process, and the similarity between the matrices and the R22 refrigerant is observed.

The last part includes infrared image processing, like the second chapter. First, the average temperature data of the evaporator and compressor inlet and outlet on the infrared image obtained for each refrigerant is obtained and then it is entered into the $\mathrm{COP_{ST}}$ process.

The system performance of the refrigeration with the PCSA and $\mathrm{COP_{ST}}$ methods in the proposed study is realized with the Matlab GUI interface (Graphical User Interfaces) given in Fig. 7. First, the infrared image of the refrigerant to be compared with the reference refrigerant is uploaded. After entering the upper and lower temperature values of the temperature bar indicators on both infrared images, the "Cut_Reference" and "Cut_Compared" buttons are pressed. Cutting is done by entering the desired coordinate points from the upper left corner and lower right corner of the images. In this way, the undesired regions such as the background parts of the test set and temperature bar indicator are cut off. In addition, temperature assignment calculations for each pixel over the so-called color infrared image are made in this section. After this process, the user is asked

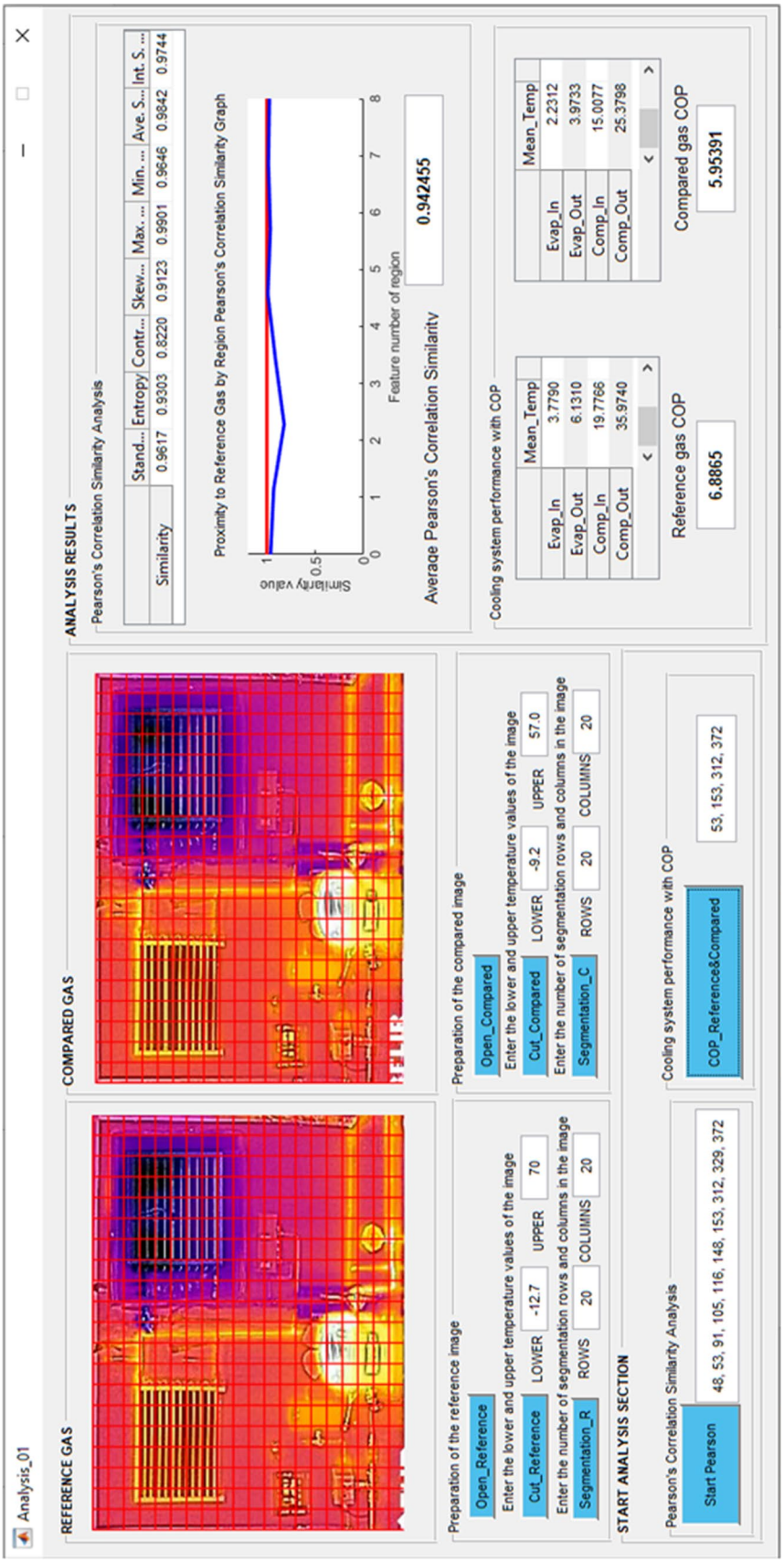

Fig. 7 Matlab GUI interface used in the study

how many sub-regions he/she should divide the cut image into and the row and column information is entered for this. In this study, the analysis was carried out by creating 400 sub-regions with all images being 20×20. By pressing the "Segmentation_R" and "Segmentation_C" buttons, the sub-regions of the display appear as updated on the interface, identified with a red line.

In the refrigeration system, 10 sub-zones were preferred for the PCSA process and 4 sub-zones were preferred for the refrigeration system performance with the COP_{ST} method. These preferred regions are given in Fig. 5 and they cover the entrance, exit and surface regions of the refrigeration system elements. The main purpose of working on only some regions, not taking the entire image, is to increase the processing speed and to focus on the analysis processes. After the user enters the region numbers, at his/her will, a comparison is made with the PCSA by pressing the "Start Pearson" button or with the COP_{ST} method by pressing the "COP_Reference and Compared" button. The analysis results of both methods are presented on the left side of the interface, in two sections, upper and lower. PCSA comparison results are graphically visualized for each feature, as well as being given as averages. In the refrigeration system performance results with the COP_{ST} method, the COP_{ST} values of the reference refrigerant and the compared refrigerant are presented together with the used region temperatures.

4 Experimental Results

In the present paper, performance analysis of R438A, R417A, R422D and R422A, which are considered as an alternative to R22, which is widely used in commercial refrigeration systems, were performed using three different methods, considering a single environmental conditions. The reason for choosing a single environment is to prevent the thermal camera from being affected by environmental disruptive external factors. Since the aim of the study and the focusing point was to perform performance analysis with a thermal camera, a single stable environment was preferred.

The method of calculating the COP value using the data from the sensors was taken as the reference for the evaluation parameter. Being other two methods using infrared imaging, PCSA and infrared surface temperature based COP_{ST} were compared with the reference method. The reference method is the parameter to evaluate the compatibility and parallelism of COP and PCSA and COP_{ST} methods.

4.1 COP Calculation Results with the Mathematical Method

The total amount of energy consumption in the experimental system includes the energy consumption of all the fans, circuit boards and compressor used in the setup. In this study where R22, R438A, R417A, R422D and R422A refrigerants were used, experiments were carried out with a vapor compression refrigeration system at ambient temperatures ranging from 20 °C to 21 °C. As a result, parameters such as compressor, condenser, evaporator capacities and COP were

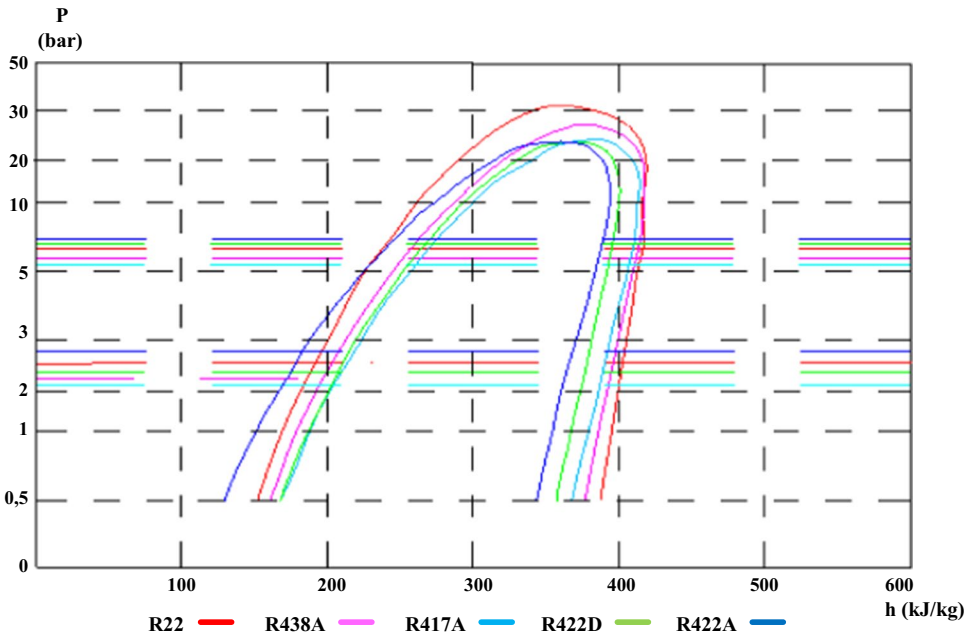

Fig. 8 Pressure-enthalpy graph for the refrigerants

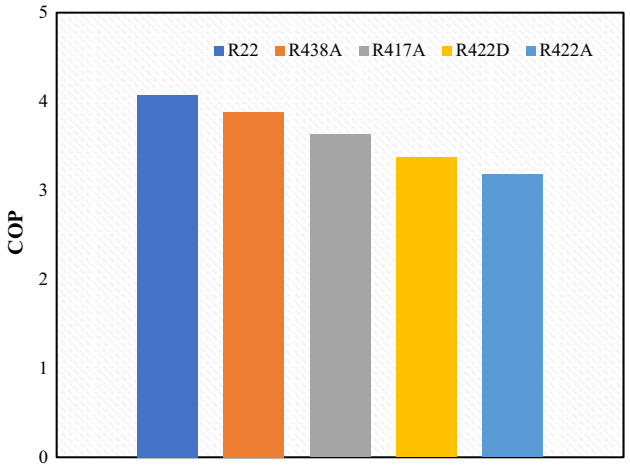

Fig. 9 Average COP change of the investigated refrigerants

calculated using the required temperature, pressure and flow measurement values. The differences and similarities that occur on the pressure-enthalpy diagrams of the refrigerants used in the study, depending on the type of refrigerant, are shown in Fig. 8. Here, in terms of evaporation, condensation pressures and enthalpy values, it is seen that R438A, R417A, R422D and R422A showed the closest performance to R22 refrigerant, respectively. It is clear that R22 has the highest critical point and a different distribution compared to other refrigerants. Besides, R417A and R438A act almost similarly. The specific refrigeration effect, defined as the enthalpy difference between the evaporator outlet and the inlet, has the greatest value when R22 is used at a certain pressure size.

None of the selected refrigerants have higher COP than R22 which ascertains that with alternative refrigerants the system energy efficiency will reduce. When the COP values in Fig. 9 are examined, it is seen that the COP value for R22 is 5% higher than that of R438A, 12% higher than that of R417A, 17% higher than that of R422D and 22% higher than that of R422A.

4.2 Experimental Results of Pearson's Correlation Similarity Analysis

The PCSA was run on 5 infrared test images taken for refrigerants PCSA, R22, R438A, R417A, R422D and R422A. After determining 10 regions for each test image and obtaining 8 features, the refrigerants were entered into PCSA process.

Table 4 gives the attribute values of the refrigerants for 10 selected regions before entering them into the PCSA process. When the numerical results are examined, it is observed that it is difficult to reach an exact result or make a comparison for the performance results of refrigerants. For this reason, before sharing the PCSA results, the comparative box graph study was conducted for the attribute data of the five refrigerants in Table 4 and for the specified regions.

Figure 10 shows the comparative box graphs of five refrigerants in terms of eight attribute values. As seen in Fig. 10a–e, refrigerants R22, R438A, R417A and R422D had similar values in terms of average. The general infrared images of the five refrigerants are in RGB format. Therefore, the color information showed very close values. Therefore, the attribute values based on color information came out close to each other. On the other hand, Fig. 10b and c shows that all refrigerants were similar in terms of upper limit. Figure 10e and f demonstrates that all the refrigerants had similar values in terms of lower limit and lower quartile. Figure 10g and h shows that the five refrigerants had similar values in terms of upper quartile, average, lower quartile and lower limit.

Especially, the ranking of the similarity of entropy, minimum temperature, average and the most intense temperature attribute data was found as R22, R438A, R417A, R422D and R422A. In addition, R417A and R422D are similar in terms of contrast, skewness and maximum temperature feature values, and R22, R417A and R422D are similar in standard deviation feature comparison. As a result, according to attribute data comparison, R438A and R417A are closer to the performance results of R22.

Figure 11 shows the comparison of the regions for five refrigerants to better test the suitability and performance of the PCSA. When the graphs are examined, it is seen that the results of R22 refrigerant have a more normal distribution in Fig. 11b d and i regions, whereas the attribute values are higher in Fig. 11a, c, f and h regions. Figure 11a, b, c, d and g confirmed the performance ranking as R22, R438A, R417A, R422D and R422A in terms of average, while Fig. 11a, f, h, i and j confirmed the ranking in terms of lower quartile and lower limit.

The visual ranking results obtained from the box graphs in Figs. 9 and 10 overlap with the results obtained after the PCSA procedure in Table 5. The results of two analyses proved the accuracy of the ranking. The proximity of R438A and R417A refrigerants in Table 4 to the R22 refrigerant was verified by the average PCSA values (0.9425 and 0.9343). As seen in Fig. 11, R422D and R422A refrigerants have high under shoot features. For this reason, the R22 refrigerant moved farther in performance than the other R438A and R417A refrigerants. It is clearly seen in Fig. 11 and Table 5 that the surface temperature features of the refrigerants used in the refrigeration system are very close to each other. This is also confirmed by the MaxT, MinT, AT and IT column data in Table 5 and the proximity of the graphs in Sects. 5, 6, 7 and 8 in Fig. 11.

Table 4 Feature data of the investigated refrigerants

Refrigerants	SD	E	C	S	MaxT	MinT	AT	IT
R22	33.068	5.723	0.506	1.189	35.375	28.669	31.982	29
	19.907	5.554	0.588	0.157	10.389	− 7.951	3.779	4
	29.834	6.345	0.478	0.120	22.677	21.686	22.580	23
	69.246	6.265	0.827	0.600	19.932	− 12.700	15.248	20
	56.886	5.819	0.835	1.802	6.161	− 7.445	− 0.096	6
	29.895	5.999	0.686	0.288	34.468	28.515	30.421	31
	42.132	6.221	0.824	0.993	8.307	− 2.496	6.131	8
	48.019	6.252	0.784	0.305	21.266	16.656	19.777	21
	13.507	5.224	0.357	− 0.332	68.297	61.734	63.989	62
	46.691	6.662	0.694	0.288	35.974	35.974	35.974	36
R438A	32.877	6.061	0.714	0.667	31.125	27.516	30.518	31
	18.656	5.572	0.369	− 0.187	9.373	− 6.308	2.231	2
	24.819	6.056	0.404	0.372	16.193	14.506	15.404	15
	75.394	6.283	0.824	0.309	20.969	− 9.200	16.163	21
	43.693	5.705	0.675	1.419	5.672	− 3.830	2.270	6
	25.959	6.042	0.663	0.242	26.797	22.512	26.154	27
	39.228	6.213	0.773	1.143	6.438	− 3.328	3.973	6
	43.307	6.183	0.780	0.333	15.990	10.653	15.008	16
	12.569	5.255	0.212	− 0.397	57.000	49.712	52.336	50
	46.129	6.595	0.702	0.366	27.651	14.553	25.380	28
R417A	33.609	6.135	0.471	0.658	32.214	25.510	30.873	32
	25.250	5.884	0.553	− 0.093	2.021	− 5.416	0.672	2
	27.026	6.265	0.486	− 0.061	20.442	12.594	16.310	17
	63.468	6.420	0.800	0.319	20.896	− 10.100	17.214	21
	50.964	5.494	0.784	1.447	3.474	− 7.130	− 0.783	3
	19.265	5.764	0.439	0.405	26.828	25.544	26.458	27
	36.591	6.076	0.725	1.320	5.448	− 2.271	3.166	5
	38.197	6.026	0.651	0.316	14.318	8.550	12.979	14
	14.365	5.294	0.298	− 0.530	51.494	47.562	48.861	48
	48.366	6.498	0.718	− 0.116	27.307	19.517	26.264	27
R422D	35.006	6.232	0.533	0.501	41.408	21.144	29.776	31
	22.410	5.824	0.471	0.186	2.292	− 9.484	− 1.947	− 1
	26.612	6.127	0.392	0.044	15.232	12.086	13.770	15
	68.953	6.368	0.808	0.235	21.089	− 11.300	17.938	21
	60.441	5.891	0.776	1.069	7.901	− 8.257	0.994	8
	19.645	5.806	0.471	− 0.414	26.362	20.899	24.798	25
	34.452	6.080	0.757	0.951	5.703	− 5.444	3.662	6
	37.565	6.260	0.682	0.673	16.286	11.742	14.875	16
	9.280	4.907	0.216	0.035	51.488	46.506	48.285	48
	48.121	6.511	0.686	0.416	28.839	24.693	28.422	29
R422A	27.640	5.740	0.427	1.215	29.557	26.534	29.012	30
	19.063	5.791	0.412	− 0.026	8.312	− 10.250	− 0.584	0
	24.107	5.963	0.478	0.333	14.498	10.565	12.800	13
	72.274	6.209	0.804	0.279	20.583	− 10.500	16.760	21
	63.205	5.763	0.788	1.217	10.219	− 5.347	5.195	10
	19.778	5.537	0.451	0.915	27.498	23.517	25.536	26
	38.324	6.229	0.749	0.982	4.911	− 7.385	2.953	5
	24.612	5.816	0.471	0.628	14.495	8.549	11.713	12
	12.643	5.093	0.243	− 0.717	54.480	49.686	51.029	50
	41.296	6.439	0.694	0.928	28.609	20.503	26.944	29

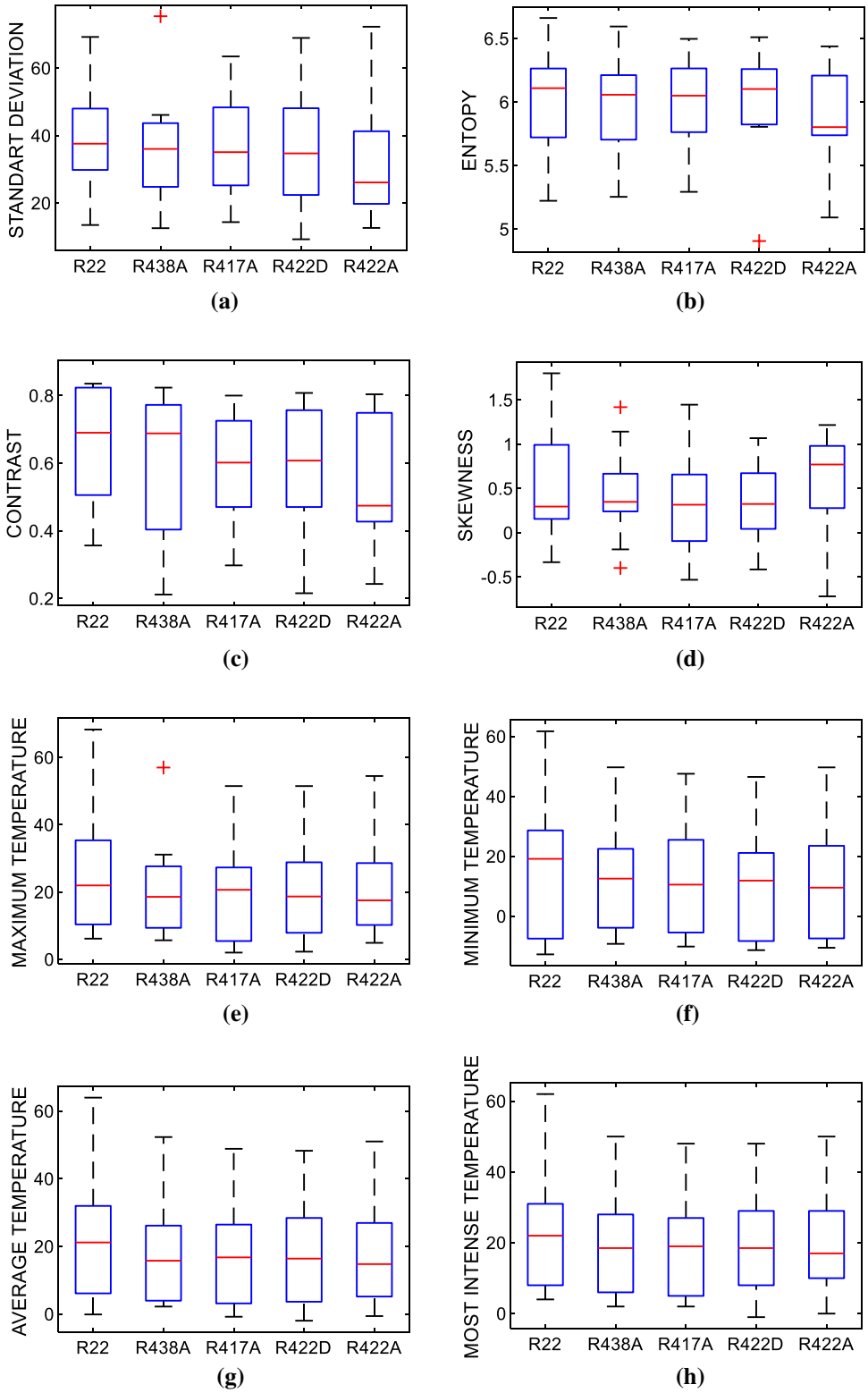

Fig. 10 Comparative box charts for feature data of R22, R438A, R417A, R422D and R422A refrigerants

4.3 Experimental Results of COP_{ST}

The evaluation of the refrigeration system performance with the COP_{ST} method is done with the surface temperature values of the evaporator inlet and outlet and the compressor inlet and outlet regions. Table 6 gives the average temperature values of these regions in addition to the COP_{ST} value of each refrigerant.

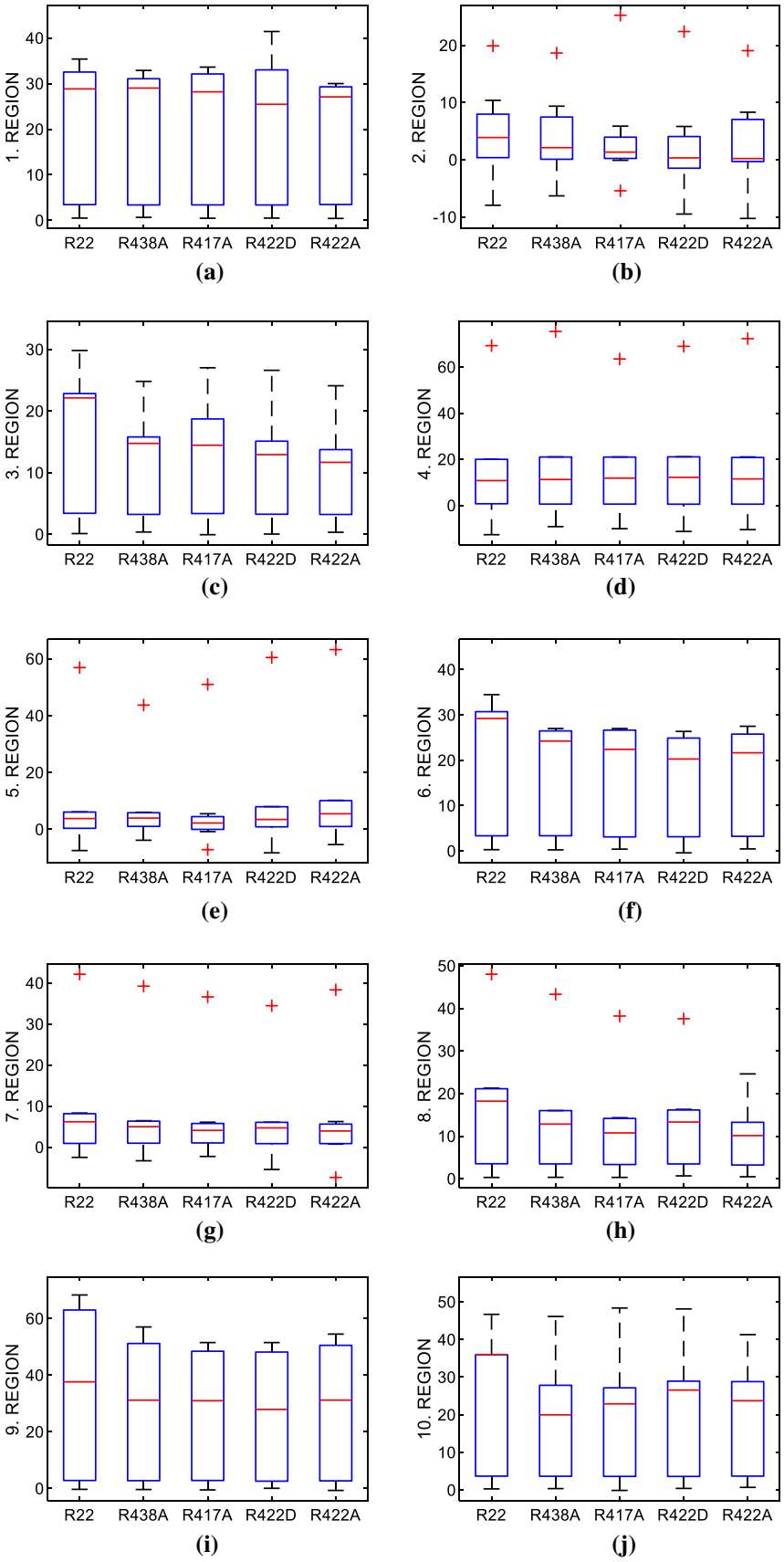

Fig. 11 Box charts of R22, R438A, R417A, R422D and R422A refrigerants in selected regions

Table 5 PCSA results of the refrigerants used

Refrigerant	PCSA results by used features								Average PCSA value
	SD	E	C	S	MaxT	MinT	AT	IT	
R22-R438A	0.9617	0.9303	0.8220	0.9123	0.9901	0.9646	0.9842	0.9744	0.9425
R22-R417A	0.9533	0.8140	0.8915	0.9154	0.9745	0.9807	0.9791	0.9661	0.9343
R22-R422D	0.9587	0.8348	0.9328	0.7286	0.9401	0.9978	0.9751	0.9653	0.9167
R22-R422A	0.9127	0.8509	0.8376	0.7727	0.9813	0.9804	0.9704	0.9577	0.9080

Table 6 COP_{ST} results of the refrigerants

Refrigerants	Evaporator input (°C)	Evaporator output (°C)	Compressor input (°C)	Compressor output (°C)	COP_{ST}
R22	3.778	6.131	19.776	35.973	6.8865
R438A	2.231	3.973	15.007	25.379	5.9539
R417A	0.671	3.165	12.978	26.263	5.3273
R422D	0.946	3.661	14.875	28.421	4.9898
R422A	−0.584	2.953	11.713	26.944	4.3057

When the numerical results in Table 6 are examined, it is seen that the performance of five refrigerants used in the study was close to each other. According to the numerical results of the COP_{ST}, the performance ranking of the refrigerants was as follows: R22, R438A, R417A, R422D and R422A. This ranking result is similar to and non-contradictory with the calculation results in 3.1. and the PCSA results in 3.2. In the four regions used in the COP_{ST}, evaporator inlet temperatures were 3.778, 2.231, 0.671, 0.946 and -0.584 as seen in Fig. 12. The ranking changed with the R417A and R422D evaporator outlet temperature values (3.165 and 3.661). Since the compressor inlet temperature of R417A was low (12.978), this refrigerant was in the third place in the ranking.

It has been determined how the system energy parameters vary according to the refrigerant types. When the COP values were examined, it was seen that R22 (4.07), R438A (3.88), R417A (3.63), R422D (3.37) and R422A (3.18) were obtained, respectively. The COP value of R22 refrigerant is 5% higher than R438A, 12% higher than R417A, 17% higher than R422D and 22% higher than R422A used as an alternative.

Figure 9, 12 and 13 show that HFC refrigerants that can be used instead of R22 in different systems and conditions have a decrease in COP values compared to systems with R22. According to the data obtained from the results, the performance ranking is R22, R38A, R417A, R422D and R422A. In the study, it is seen that the results obtained with these three methods are compatible with similar studies in the literature. In addition to the mathematical examination of R417A, R438A, R422A and R422D refrigerants in a commercial refrigeration system operating with R22, the use of infrared thermal imaging and PCSA and COP_{ST} methods reveals the originality of the study.

One of the main objectives of the study, refrigerants that do not damage the ozone layer, which are widely used in refrigeration systems, will be preferred. In this way, it will be

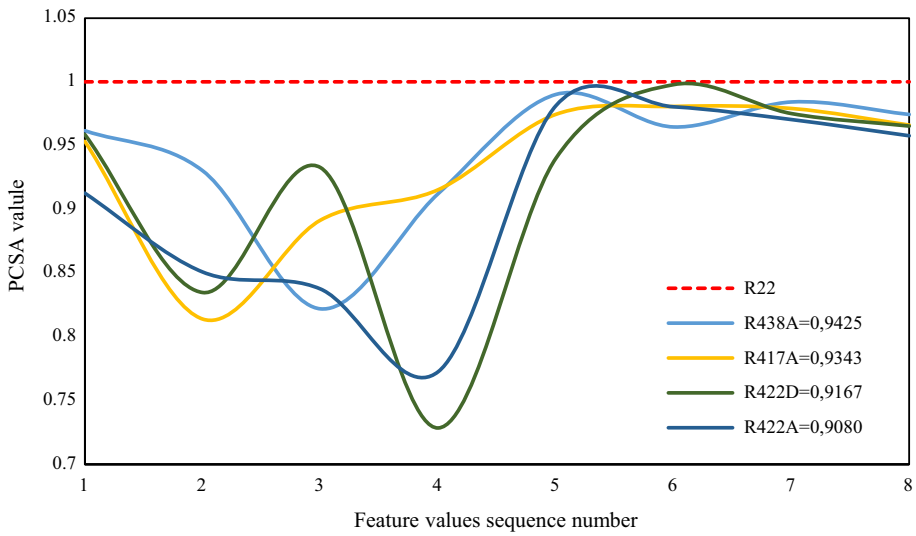

Fig. 12 Comparison of R22 with other refrigerants R438A, R417A, R422D and R422A using PCSA method

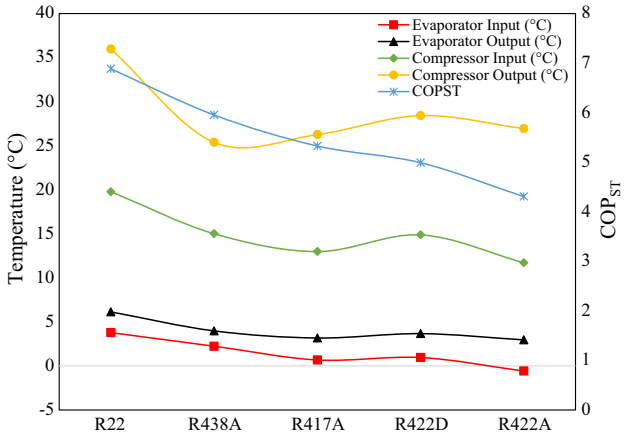

Fig. 13 Comparison of R22, R438A, R417A, R422D and R422A refrigerants using COP_{ST} method

possible to decide on the refrigerant consuming less energy for the appropriate temperature.

In this study, the examination of PCSA and COP_{ST} methods applied using infrared image processing technique contributed to the literature by providing a different perspective.

5 Conclusions

In the proposed study, the performance analysis of R438A, R417A, R422D and R422A refrigerants, which are considered as an alternative to R22 refrigerant, which is widely used in commercial refrigeration systems, was performed using three different methods. These methods are the inclusion of temperature and pressure data from sensors into the COP calculation process, PCSA using infrared imaging, and COP_{ST} based on infrared surface temperature.

It was proven that the mathematical calculation method of the COP value and the ranking compatibility of the experimental results obtained from the PCSA and COP_{ST} methods can be successfully performed remote performance analysis of the refrigeration system thanks to the infrared imaging. PCSA values show their proximity to R22 refrigerant with values of R438A (0.9425), R417A (0.9343), R422D (0.9167) and R422A (0.9080). Likewise, the data of R22 (6.8865), R438A (5.9539), R417A (5.3273), R422D (4.9898) and R422A (4.3057) were obtained with the COPST method, and it was ranked in the same order with the other two methods. It was demonstrated that it is applicable in the evaluation of performance test with the developed infrared image processing. When the experimental results are examined, it shows that each of the alternative refrigerants is a good replacement and regeneration refrigerant for R22, and the most suitable ones according to R22 are R417A and R438A. In terms of performance, one of the biggest reasons why R422A, R422D, R417A and R438A are not a good alternative is their high power consumption at low temperatures.As a result, the study revealed that R438A is the best among the refrigerants developed as an alternative to R22.

With the infrared imaging used in the study, sensor installation, cost and wiring problems have been eliminated, and sensor installation and wiring have become more visual with the interface feature. The software developed for the system is easily programmable for the user and has the ability to record and draw graphs simultaneously.

Acknowledgements This study was supported by The Scientific and Technological Research Council of Turkey (TÜBİTAK) with the project number 218M936.

References

1. Aprea, C.; Renno, C.: Experimental comparison of R22 with R417A performance in a vapour compression refrigeration plant subjected to a cold store. Energy Convers. Manag. **45**(11–12), 1807–1819 (2004)
2. Torrella, E.; Cabello, R.; Sanchez, D.; Larumbe, J.A.; Llopis, R.: On-site study of HCFC-22 substitution for HFC non-azeotropic blends (R417A, R422D) on a water chiller of a centralized HVAC system. Energy Build. **42**(9), 1561–1566 (2010)
3. La. Rocca, V.; Panno, G.: Experimental performance evaluation of a vapour compression refrigerating plant when replacing R22 with alternative refrigerants. Appl. Energy. **88**(8), 2809–2815 (2011)
4. Elgendy, E.; Hassanain, M.; Fatouh, M.: Assessment of R-438A as a retrofit refrigerant for R-22 in direct expansion water chiller. Int. J. Refrig. **50**, 127–136 (2015)
5. Saeed, M.U.; Qureshi, S.R.; Hashmi, K.J.; Khan, M.A.; Danish, S.N.: Performance assessment of alternate refrigerants for retrofitting R22 based air conditioning system. Therm. Sci. **22**(2), 931–941 (2018)
6. Ergün, A.; Gürel, A.E.; Ceylan, İ: Ticari soğutma sistemlerinde R22 akışkanının alternatifi olarak R438A ve R417A akışkanlarının performansının incelenmesi. Gazi Üniv. Fen Bilimleri Dergisi Part C Tasarım ve Teknol. **6**(4), 824–833 (2018)
7. Cingiz, Z.; Katırcıoğlu, F.; Çay, Y.; Kolip, A.: Buhar sikiştirmali soğutma sisteminde R22 alternatifi soğutucu akişkanlarin termodinamik analizi. Politek. Derg. (2019). https://doi.org/10.2339/politeknik.548115
8. United States Environmental Protection Agency, Significant new alternatives policy (SNAP) program (2020). https://www.epa.gov/snap
9. Erham, E; Inten, R.N.: Design of a new online monitoring system of COP based on Arduino Uno with application to split A/C. IOP Conf. Ser. Mater. Sci. Eng. **830**(4), 042030 (2020)
10. Chown, G.A.; Burn, K.N.: Thermographic Identification of Building Enclosure Effects and Deficiencies, Canadian Building Digest, CBD-229. Institute for Research in Construction, National Research Council Canada (1983)
11. Balaras, C.A.; Argiriou, A.A.: Infrared thermography for building diagnostics. Energy Build. **34**, 171–183 (2002)
12. Al-Kassir, A.R.; Fernandez, J.; Tinaut, F.V.; Castro, F.: Thermographic study of energetic installations. Appl. Therm. Eng. **25**, 183–190 (2005)
13. Avdelidis, N.P.; Moropoulou, A.: Emissivity measurements on historic building materials using dual wavelength infrared

thermography. Thermosense XXIII, SPIE Press, Orlando, Florida, USA, pp. 224–228 (2001)
14. Datcu, S.; Ibos, L.; Candau, Y.; Mattei, S.: Improvement of building wall surface temperature measurements by infrared thermography. Infrared Phys. Technol. **46**, 451–467 (2005)
15. Grinzato, E.; Vavilov, V.; Kuppinen, T.: Quantitative infrared thermography in buildings. Energy Build. **29**, 1–9 (1998)
16. Carignano M.; Pipplone, E. Optimization of windscreen defrosting for industrial vehicles via computer assisted thermographic analysis. SAE Technical Paper 905237 (1990)
17. Burch, S.; Hassani, V.; Penney, T.: Use of infrared thermography for automotive climate control analysis. In: Vehicle Thermal Management Systems Conference, Colombus, Ohio, 921136 (1994)
18. Boukhanouf, R.; Haddad, A.; North, M.T.; Buffone, C.: Experimental investigation of a flat plate heat pipe performance using IR thermal imaging camera. Appl. Therm. Eng. **26**(17–18), 2148–2156 (2006)
19. Freund, S.; Pautsch, A.G.; Shedd, T.A.; Kabelac, S.: Local heat transfer coefficients in spray cooling systems measured with temperature oscillation IR thermography. Int. J. Heat Mass Transf. **50**(9–10), 1953–1962 (2007)
20. Korukçu, M.Ö.; Kilic, M.: The usage of IR thermography for the temperature measurements inside an automobile cabin. Int. Commun. Heat Mass Transf. **36**(8), 872–877 (2009)
21. Snekhalatha, U.; Anburajan, M.; Venkatraman, B.; Menaka, M.; Raj, B. Evaluation of rheumatoid arthritis in small animal model using Thermal imaging. In: International Conference on Signal Processing, Communication, Computing and Networking Technologies, pp. 785–791 (2011)
22. Pan, C.Y.; Huang, C.S.; Horng, G.J.; Peng, P.L.; Jong, G.J.: Infrared image processing for a physiological information telemetry system. Wirel. Pers. Commun. **83**(4), 3181–3208 (2015)
23. Weinmann, M.; Leitloff, J.; Hoegner, L.; Jutzi, B.; Stilla, U.; Hinz, S.: Thermal 3D mapping for object detection in dynamic scenes. ISPRS Ann. Photogramm. Remote Sens. Spat. Inf. Sci. **2**(1), 53–60 (2014)
24. Righetti, G.; Zilio, C.; Longo, G.A.: Comparative performance analysis of the low GWP refrigerants HFO1234yf, HFO1234ze (E) and HC600a inside a roll-bond evaporator. Int. J. Refrig. **54**, 1–9 (2015)
25. Taheri-Garavand, A.; Ahmadi, H.; Omid, M.; Mohtasebi, S.S.; Mollazade, K.; Smith, A.R.; Carlomagno, G.M.: An intelligent approach for cooling radiator fault diagnosis based on infrared thermal image processing technique. Appl. Therm. Eng. **87**, 434–443 (2015)
26. Jin, S.; Hrnjak, P.: Refrigerant and lubricant charge in air condition heat exchangers: Experimentally validated model. Int. J. Refrig. **67**, 395–407 (2016)
27. Katırcıoğlu, F.; Çay, Y.; Cingiz, Z.: Infrared image enhancement model based on gravitational force and lateral inhibition networks. Infrared Phys. Technol. **100**, 15–27 (2019)
28. Kim, H.: A knowledge based infrared camera system for invisible gas detection utilizing image processing techniques. J. Ambient Intell. Hum. Comput. 1–11 2019
29. Katırcıoğlu, F.: Real-time infrared image processing for control and monitoring of greenhouse system. J. Appl. Remote Sens. **14**(2), 026503 (2020)
30. Linde, Linde gas (2020) https://www.linde-gas.com/en/products_and_supply/refrigerants/hcfc_refrigerants/r22/index.html. Accessed 26 May 2020
31. Bock Compressor, Bock Compressor, Alternative Refrigerants Information on use of R22 (2020). http://www.bock.de/media/files/PDF/Produktinformationen/96151_Alternative-refrigerants_R22_Gb.pdf. Accessed 16 Apr 2020
32. Climalife IDS Refrigeration Limited, climalife IDS Refrigeration Limited; Available: https://www.climalife.co.uk/docs/ISCEON-MO29-Retrofit-Guidelines-V2.pdf. 15 Nisan 2020 (2020)
33. Allgood, C.C.; Lawson, C.C.: Performance of R-438A in R-22 refrigeration and air conditioning systems. In: International Refrigeration and Air Conditioning Conference, Indiana, USA, Purdue University, pp. 1–8 (2010)
34. Gürel, A.E.; Ağbulut, Ü.; Ergün, A.; Yıldız, G.: Energy, Exergy and Environmental (3E) assessments of various refrigerants in the refrigeration systems with internal heat exchanger. Heat Transf. Res. **51**(11), 1029–1041 (2020)
35. Akpınar, H.: Data Veri Madenciliği-Veri analizi. Papatya, Istanbul (2014)
36. Ahlgren, P.; Jarneving, B.; Rousseau, R.: Requirements for a cocitation similarity measure, with special reference to Pearson's correlation coefficient. J. Am. Soc. Inform. Sci. Technol. **54**(6), 550–560 (2003)
37. Jiang, H.; Zeng, L.; Bi, B.: A comprehensive method of contour extraction for industrial computed tomography images. Opt. Lasers Eng. **51**(3), 286–293 (2013)
38. Duan, L.; Yao, M.; Wang, J.; Bai, T.; Zhang, L.: Segmented infrared image analysis for rotating machinery fault diagnosis. Infrared Phys. Technol. **77**, 267–276 (2016)
39. Barbieri, A.L.; De. Arruda, G.F.; Rodrigues, F.A.; Bruno, O.M.; da Fontoura Costa, L.: An entropy-based approach to automatic image segmentation of satellite images. Phys. A **390**(3), 512–518 (2011)
40. Simone, G.; Pedersen, M.; Hardeberg, J.Y.: Measuring perceptual contrast in digital images. J. Vis. Commun. Image Represent. **23**(3), 491–506 (2012)
41. Yıldız, G.; Ağbulut, Ü.; Gürel, A.E.: A review of stability, thermophysical properties and impact of using nanofluids on the performance of refrigeration systems. Int. J. Refrig. (2021). https://doi.org/10.1016/j.ijrefrig.2021.05.016